Near-Critical Behavior of the Dynamic Stress-Optical Coefficient in Liquid Crystalline Elastomers

R. Sigel,* W. Stille, G. Strobl, and R. Lehnert

Fakultät für Physik, Universität Freiburg, Hermann-Herder-Strasse 3, 7800 Freiburg, Germany

Received February 2, 1993; Revised Manuscript Received May 11, 1993

ABSTRACT: Dynamic stress-optical measurements on liquid crystalline elastomers with different cross-linking densities have been carried out in the isotropic phase. The appearance of two relaxation processes in the spectra is probably due to the side-on attachment of the spacers to the mesogenic groups. The relaxation frequencies and the relaxation strengths of the processes show critical behavior in qualitative agreement with the Landau-de Gennes theory. The strong cross-linking density dependence of the relaxation strengths provides evidence that the cross-linking points locally perturb the liquid crystalline order. A comparison of the dynamic mechanical and the dynamic stress-optical behavior of the samples indicates that the stress-optical processes are triggered by fast contributions to the mechanical spectrum.

Introduction

Liquid crystalline elastomers combine the properties of polymer networks and liquid crystals. Due to the existing elastic network a mechanical stress cannot relax by flow processes and therefore affects the liquid crystalline order permanently. Applying a mechanical field, a nematic polydomain structure can be transformed into a monodomain texture. In the isotropic phase the stress causes a nonzero order parameter and a shift in the nematic–isotropic phase transition temperature T_{NI}.[1] The effect of a mechanical field on the liquid crystalline order is much stronger than the effect of experimentally realizable electric or magnetic fields.[2] Like all susceptibilities related to the order parameter S, as, for example, the Kerr and the Cotton–Mouton constant, the stress-optical coefficient shows a strong increase as the temperature approaches the transition temperature T_{NI} in the isotropic phase. The increase is described by the Landau–de Gennes theory as a "near-critical" behavior.[3-7] The critical point T^* where the divergence would occur is located slightly below T_{NI}, so that the phase transition interferes before T^* is reached.

Critical behavior is always associated with a critical slowing down of the order parameter dynamics. As reported in this paper, critical dynamics in liquid crystalline elastomers is in fact observed. We have performed measurements of the dynamic stress-optical coefficient in the frequency range $0.1 \leq f \leq 50$ Hz. In addition, by measuring dynamic mechanical and dynamic stress-optical properties of the sample simultaneously, details of the interaction between the network and mesogens can be studied. Similar measurements were first performed in the groups of Read,[8] Stein,[9] and Kawai[10] in studies of semicrystalline and amorphous polymers.

In the following, first the samples under study and the experimental setup are described. Then we present the dynamic mechanical and dynamic stress-optical measurements, which were performed in the isotropic phase, and discuss them in the last section.

Experimental Section

Samples. The liquid crystalline elastomers were synthesized and characterized in the group of Prof. H. Finkelmann, Institut für Makromolekulare Chemie, Universität Freiburg. Figure 1 shows their chemical structure. The mesogenic groups R_1 and R_2 are attached laterally to the polymethacrylate backbone via spacers of six methylene groups. The junction point of the spacer is in the central part of the mesogen. A low fraction (y) of the mesogens contains cyano end groups (to enable a determination of the order parameter by IR dichroism measurements).

We examined two elastomers, LCE-1 and LCE-5, which differ only in their cross-linking density. Their structural features and phase behavior are shown in Table I. The numbers "1" and "5" in the denominations of the samples refer to their cross-linking densities: the cross-linking density of the second sample is about 5 times as high as the cross-linking density of the first sample. In comparison to the theoretical maximal cross-linking densities anticipated from the fractions of the used cross-linking agent, the actually realized cross-linking densities were much lower. They were derived from stress–strain measurements and followed from N_M, the average number of monomer units between two cross-linking points. This fact indicates that the cross-linking reaction was incomplete or that many cross-links are not mechanically active.

Apparatus. Dynamic optical and mechanical measurements probe the temperature and frequency dependence of the mechanical and optical properties of a sample. In the experiment the sample is exposed to a stress

$$\sigma(t) = \sigma_0 + \sigma_1 e^{i\omega t} \tag{1}$$

which consists of a static component σ_0 applied to stretch the sample and a superposed sinusoidal modulated dynamic component σ_1 with frequency $f = \omega/2\pi$ (σ, σ_0, and σ_1 are engineering stresses, i.e., the applied force per cross-section area in the unstrained state). The stress causes a strain

$$\epsilon(t) = \epsilon_0 + \epsilon_1 e^{i(\omega t - \delta)} \tag{2}$$

and a birefringence

$$\Delta n(t) = \Delta n_0 + \Delta n_1 e^{i(\omega t - \varphi)} \tag{3}$$

in the sample, where ϵ_0, ϵ_1, Δn_0, and Δn_1 are the zeroth and the first Fourier components of the strain and the birefringence, respectively, and δ and φ are phase angles. The dynamic mechanical properties of the sample will be described by the complex elastic modulus

$$E^* = E' + iE'' \frac{\sigma(t) - \sigma_0}{\epsilon(t) - \epsilon_0} = \frac{\sigma_1}{\epsilon_1} e^{i\delta} \tag{4}$$

and the dynamic stress-optical behavior will be characterized by

0024-9297/93/2226-4226$04.00/0

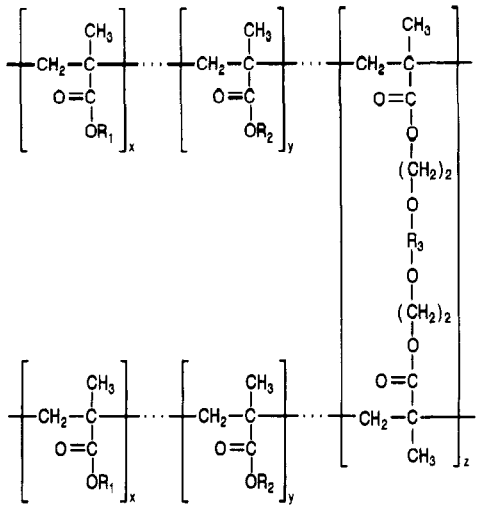

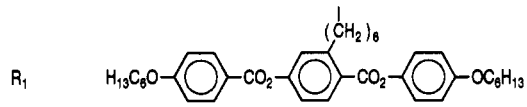

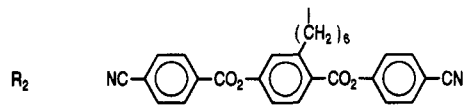

Figure 1. Chemical structure of the samples. The stoichiometric fractions x, y, and z are listed in Table I.

Table I. Chemical Structure and Phase Behavior of the Elastomers

sample	x	y	z	N_M[a]	T_g,[b] °C	T_{NI}[c], °C
LCE-1	0.935	0.015	0.050	200	30	59.1
LCE-5	0.795	0.015	0.190	41	34	60.4

[a] N_M: average number of monomer units between two cross-linking points, derived from stress–strain measurements. [b] Glass transition temperature T_g, obtained by DSC. [c] Nematic–isotropic phase transition temperature T_{NI}, derived from the change in the apparent extinction of the sample.

the dynamic stress-optical coefficient[11]

$$C^* = C' - iC'' \frac{\Delta n(t) - \Delta n_0}{(\sigma(t) - \sigma_0)(1 + \epsilon_0)} = \frac{\Delta n_1}{\sigma_1(1 + \epsilon_0)} e^{-i\varphi} \qquad (5)$$

As in the case of ordinary rubbers, the stress-optical coefficient is calculated with the component of the true stress $\sigma_1(1 + \epsilon_0)$, which is given by the applied force per cross-section area in the strained state (the small contribution of ϵ_1 is neglected).[12]

The experimental apparatus consists of a commercial mechanical spectrometer (Polymer Laboratories DMTA MK II) working in tensile geometry, with the additional implementation of an optical setup for a simultaneous determination of the birefringence. Eleven frequencies of the spectrometer in the range $0.1 \le f \le 50$ Hz are available. Figure 2 shows the optical setup. A sample is placed between two crossed polarizers, oriented with their axes at angles of +45 and −45° with regard to the optical axis of the sample, which coincides with the tensile axis. The beam of a He–Ne laser passes the polarizers and the sample and is detected by a photodiode.

The transmitted intensity I as a function of the birefringence Δn and thickness d of the sample is given by

$$I(\Delta n) = \frac{I_{max}}{2}\left(1 - \cos\left(2\pi\Delta n \frac{d}{\lambda}\right)\right) \qquad (6)$$

where I_{max} is the maximum of the transmitted intensity and λ is the wavelength of the laser light (633 nm). The birefringence $\Delta n(t)$ is given by eq 3. To get a sinusoidal modulated intensity in the case of a sinusoidal modulated birefringence, σ_0 is chosen

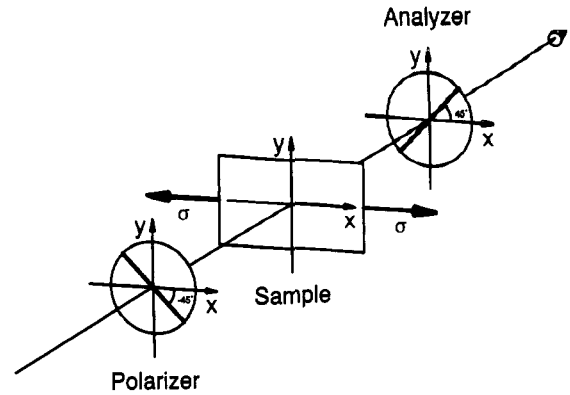

Figure 2. Optical setup to determine the birefringence of the sample simultaneously with the mechanical characterization.

in such a way that Δn_0 fulfills the equation

$$2\pi\Delta n_0 \frac{d}{\lambda} = \frac{\pi}{2} \qquad (7)$$

i.e.

$$\Delta n_0 = \frac{\lambda}{4d} \qquad (8)$$

Around this value of Δn_0, the *operating point*, the cosine function in eq 6 is approximately linear. First-order Taylor expansion of eq 6 around the operating point leads to

$$I(\Delta n) \approx \frac{I_{max}}{2}\left(1 + 2\pi\Delta n \frac{d}{\lambda}\right) \qquad (9)$$

Combination of the eqs 9, 3, and 8 results in

$$I(t) \approx \frac{I_{max}}{2}\left(1 + 2\pi \frac{d}{\lambda}\Delta n_1 e^{i(\omega t - \varphi)}\right) \qquad (10)$$

Hence, for a small sinusoidal modulation of Δn around the operating point, the amplitude Δn_1 and the phase angle φ of the dynamical component of the birefringence can be determined by a measurement of the amplitude and the phase angle of the intensity signal.

In the experiment the operating point is stabilized by controlling the static stress component, keeping the average intensity constant ($\bar{I} = I_{max}/2$). The intensity of the transmitted light and the strain of the sample are sampled simultaneously at 64 equidistant points per period. Fast Fourier transformation on the controlling microcomputer yields the amplitudes ϵ_1 and Δn_1 of strain and birefringence and their relative phase angle $\psi = (\varphi - \delta)$. Using the elastic modulus measured by the mechanical spectrometer, C^* can be calculated using eqs 4 and 5. It is an inherent problem of the method that the noise in the mechanical data is transferred to the stress-optical coefficient.

Results

Mechanical Properties. The temperature dependences of the real part of the dynamic elastic modulus E' and of the loss factor $\tan(\delta)$, measured at a frequency of 30 Hz, are shown in Figure 3. The decrease of $\log(E')$ and the maximum of $\tan(\delta)$ indicate the broad dynamic glass transition of the samples. For low temperatures $\log(E')$ approaches the glass modulus, which is independent of the cross-linking density; at high temperatures E' approaches the rubber value, which is proportional to the cross-linking density. Note that at the chosen frequency there is no noticeable change in the dynamic mechanical data at the nematic–isotropic phase transition; T_{NI} is located at 60 °C.

In contrast to the dynamical behavior, there is a distinct change in length of the samples at T_{NI}, as shown in Figure 4. During the mechanical measurement, the static component of the stress is kept constant. Hence, the change in length of the samples originates from the change of the

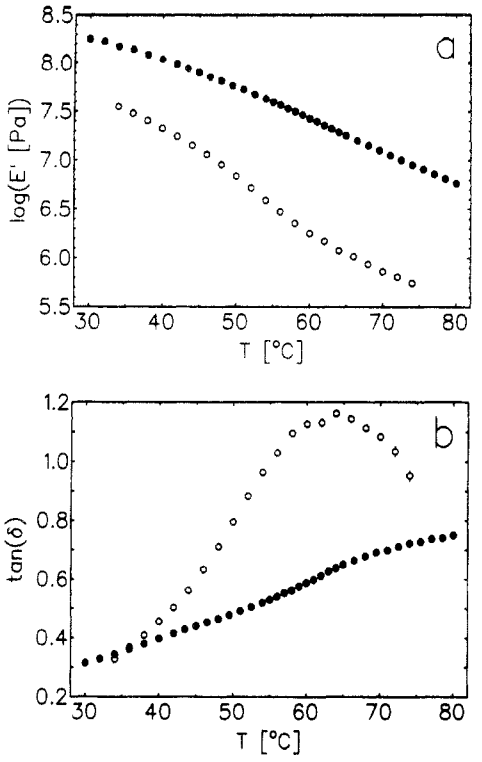

Figure 3. Temperature dependence of log (E') (a) and tan(δ) (b) for LCE-1 (○) and for LCE-5 (●), measured at 30 Hz.

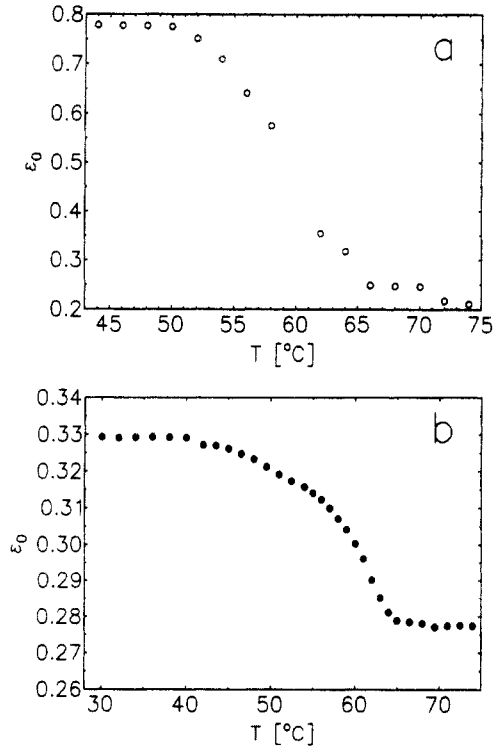

Figure 4. Static strain of LCE-1 (a) and LCE-5 (b) under constant stress during the mechanical measurement. The change in length is due to the change in the order parameter.

order parameter. To avoid a perturbation of the measurement introduced by the lengthening, a delay of at least 0.5 h was inserted between two successive measurements. The extent of the length increase is strongly dependent on the cross-linking density: the weaker cross-linked sample LCE-1 showed a much higher lengthening than the stronger cross-linked sample LCE-5.

Dynamic Stress-Optical Coefficient. Frequency spectra of the dynamic stress-optical coefficient of the samples are shown in Figures 5 (LCE-1) and 6 (LCE-5).

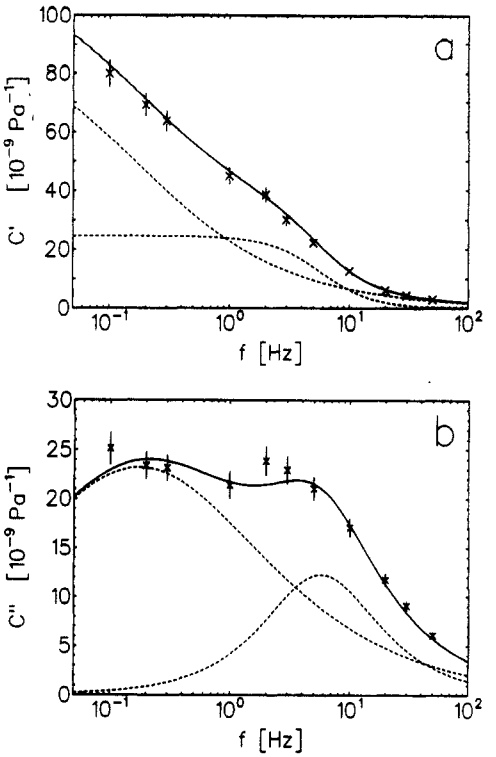

Figure 5. Frequency spectrum of the stress-optical coefficient $C^* = C' - iC''$ of LCE-1 at 65 °C (a, C'; b, C''). A faster Debye process and a slower Cole–Cole process are simultaneously fitted to C' and C''.

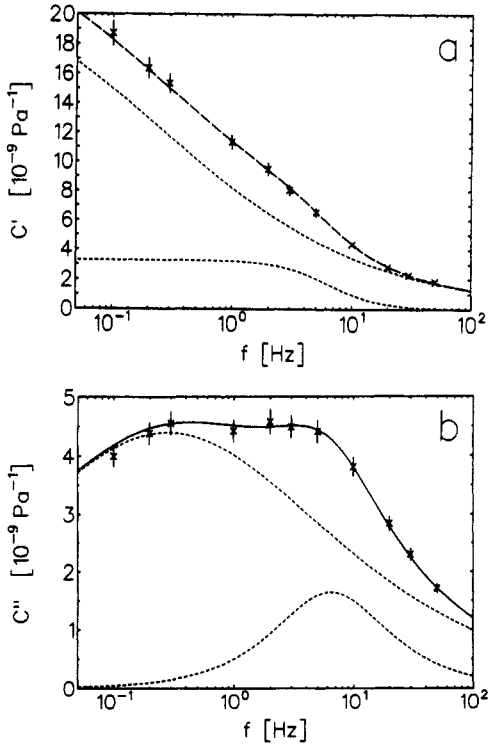

Figure 6. Frequency spectrum of the stress-optical coefficient $C^* = C' - iC''$ of LCE-5 at 65 °C (a, C'; b, C''). A faster Debye process and a slower Cole–Cole process are simultaneously fitted to C' and C''.

They were measured at a temperature of 65 °C, a few degrees above T_{NI}. To evaluate the spectra, the sum of two relaxation processes $C^* = C^*_{fast} + C^*_{slow}$ was fitted to the data: a fast Debye process

$$C^*_{fast}(f) = \frac{\Delta C_{fast}}{1 + if/f_{fast}} \tag{11}$$

and a slower, broader Cole–Cole process[13]

$$C^*_{slow}(f) = \frac{\Delta C_{slow}}{1 + (if/f_{slow})^{1-\alpha}} \quad (12)$$

The adjusted parameters are the relaxation frequencies f_{slow} and f_{fast}, the relaxation strengths ΔC_{slow} and ΔC_{fast}, and the parameter α, which characterizes the width of the slower process. Fortunately, both relaxation processes showed up in the limited frequency window of the mechanical spectrometer. To improve the accuracy of the parameters, the spectra of C' and C'' were fitted simultaneously, so that the five unknown parameters were adjusted by use of 22 data points.

The temperature dependences of the relaxation frequencies and relaxation strengths are represented in Figures 7 (LCE-1) and 8(LCE-5). For both samples, the two relaxation processes show a critical behavior: approaching the clearing point from high temperatures, the relaxation strengths diverge and the relaxation frequencies show a critical slowing down. The large error bars of f_{slow} and ΔC_{slow} originate from the fact that only half of the slow relaxation process lies in the frequency window of the apparatus (refer to Figures 5 and 6). To describe the temperature dependence of the relaxation strength, the equation

$$\Delta C(T) = \frac{A}{T - T_N^*} + \Delta C_0 \quad (13)$$

was fitted to the data. Equation 13 corresponds to eq 28 given in the next section, with an additional contribution ΔC_0 accounting for a temperature-independent background. In the case of the relaxation frequencies of LCE-1, straight lines

$$f(T) = M(T - T_N^*) \quad (14)$$

corresponding to eq 27 (next section) could be fitted to the data. The derived fit parameters are given in Table II.

The data of LCE-1 were obtained in two different measurements; the measurement in the temperature range $59 \le T < 63.5$ °C was performed much later than a first measurement in the range $62 \le T \le 72$ °C. In Figure 7c, showing f_{fast}, a slight shift between the two data sets is visible. A probable reason for this shift is a lowering of the clearing temperature, caused by a partial chemical decomposition of the sample. For the fitting of eq 14 to the data, only the measurement near T_{NI} (×) is used.

Comparison of Figures 7 and 8 allows conclusions about the effect of the cross-linking density on relaxation frequencies and relaxation strengths. While the values of f_{slow} in Figures 7a and 8a as well as the values of f_{fast} in Figures 7c and 8c are quite similar, there is a strong effect of the cross-linking density on the relaxation strengths. Comparison of Figures 7b and 8b and of Figures 7d and 8d shows that the relaxation strengths ΔC_{slow} and ΔC_{fast} are much stronger in the case of the lower cross-linked sample LCE-1 than in the case of the higher cross-linked sample LCE-5. Hence, it was found that relaxation frequencies show only a weak dependence on the cross-linking density, while there is a strong effect of the cross-linking density on the relaxation strengths.

Phase Shift between Strain and Birefringence. A peculiar result of the measurement is shown in Figure 9. The phase shift $\psi = \varphi - \delta$ between strain and birefringence signal can be positive as well as negative. At first sight a negative sign of this phase means that the sample becomes birefringent before it is strained. Obviously, the simple picture that a stress applied to the sample first causes a strain in the network, which subsequently affects the liquid crystalline order and therefore the birefringence, has to be modified. We shall come back to this point in the discussion.

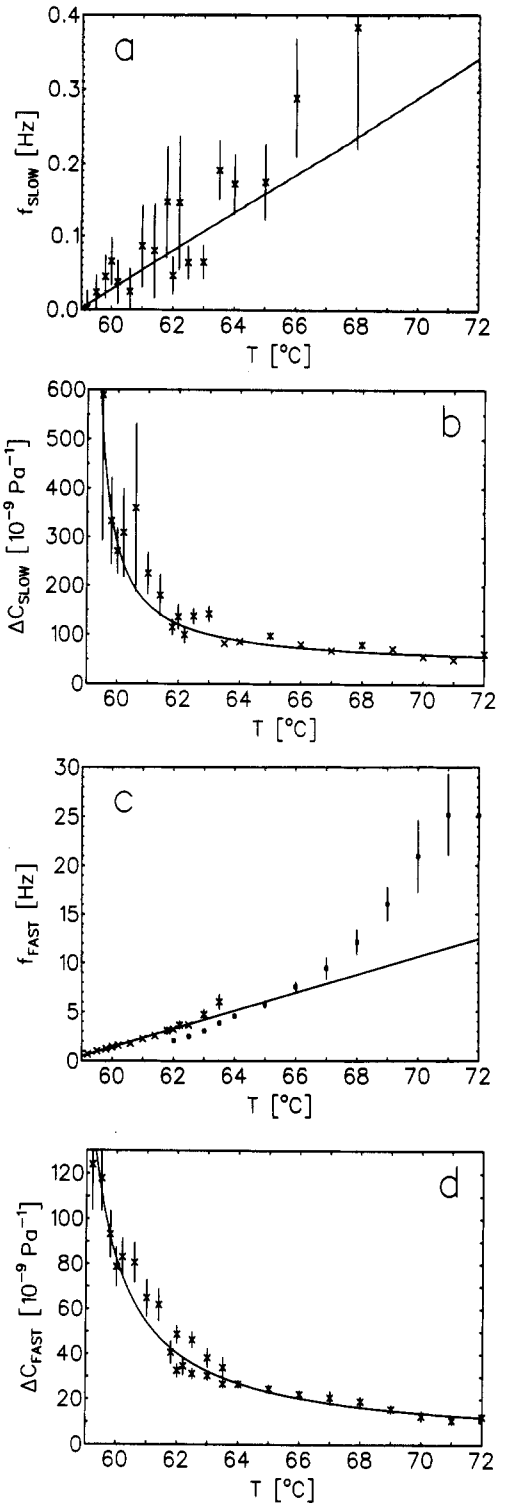

Figure 7. Temperature dependence of the relaxation frequencies and strengths f_{slow} (a), ΔC_{slow} (b), f_{fast} (c), and ΔC_{fast} (d) of LCE-1 as derived from the curve fitting.

Discussion

Landau–de Gennes Theory. The results are discussed within the scope of the Landau–de Gennes theory.[3-7] De Gennes described the free energy density f of a nematic liquid crystal in the neighborhood of the nematic–isotropic

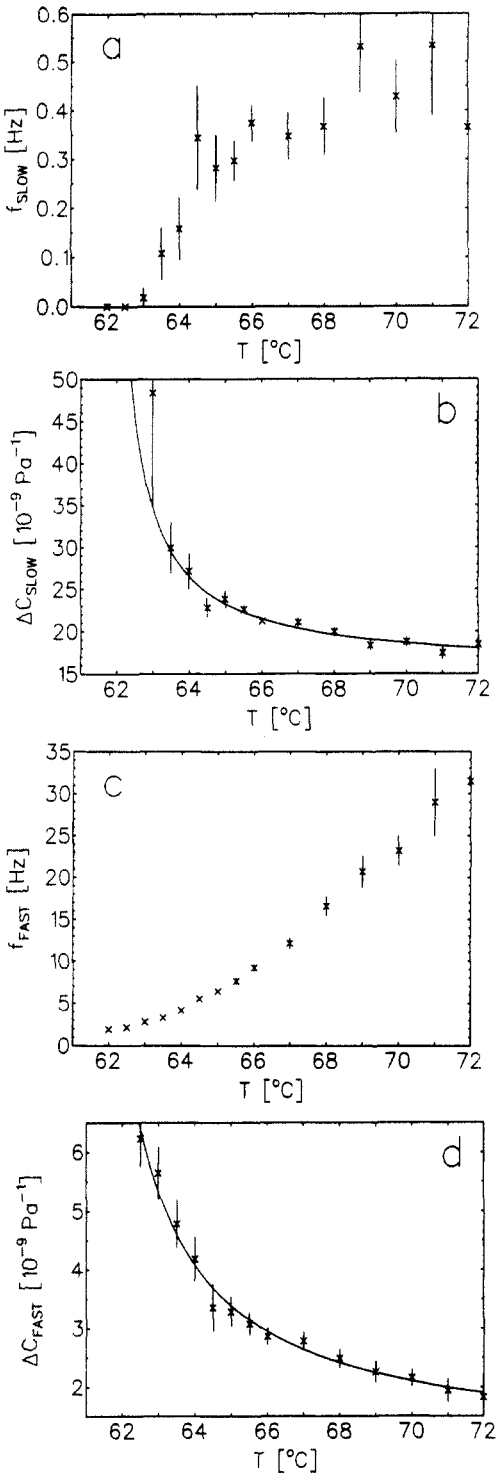

Figure 8. Temperature dependence of the relaxation frequencies and strengths f_{slow} (a), ΔC_{slow} (b), f_{fast} (c), and ΔC_{fast} (d) of LCE-5 as derived from the curve fitting.

phase transition as a power series in the order parameter S

$$f = f_0 + \frac{A}{2}S^2 - \frac{B}{3}S^3 + \frac{C}{4}S^4 \quad (15)$$

where the value of S in thermodynamic equilibrium is derived by minimizing f with respect to S. Due to the symmetry there exists no linear term in S. The coefficients B and C are only weakly temperature dependent and therefore assumed as constant. The characteristic feature is the temperature dependence of A, given by

$$A(T) = a(T - T^*) \quad (16)$$

with a denoting a temperature-independent constant. The temperature T^* is located slightly below the nematic–isotropic phase transition and can be determined by investigating the near-critical behavior of the liquid crystal in the isotropic phase: the mesogens behave in the isotropic phase as if there would be a second-order phase transition at T^*.

To describe liquid crystalline elastomers, de Gennes extended eq 15 by additional terms, leading to[5]

$$f = f_0 + \frac{A}{2}S^2 - \frac{B}{3}S^3 + \frac{C}{4}S^4 - US\epsilon + \frac{1}{2}E\epsilon^2 - \sigma\epsilon \quad (17)$$

where σ is the applied stress, ϵ the strain of the sample, E the static elastic modulus, and U the coupling constant between strain and order parameter. The equilibrium values of S and ϵ are again calculated by minimizing eq 17 with respect to S and ϵ. Minimization of f in eq 17 with respect to ϵ leads to

$$\epsilon_{eq} = \frac{1}{E}\sigma + \frac{U}{E}S \quad (18)$$

In addition to the applied stress, the liquid crystalline order can also affect the strain of the sample. Even if there is no external stress, a spontaneous deformation of the network occurs in the nematic phase.[14] Inserting eq 18 in eq 17 results in

$$f = f_0 - \frac{U}{E}\sigma S + \frac{a}{2}(T - T_N^*)S^2 - \frac{B}{3}S^3 + \frac{C}{4}S^4 - \frac{\sigma^2}{2E} \quad (19)$$

where T_N^* is given by

$$T_N^* = T^* + \frac{U^2}{Ea} \quad (20)$$

T_N^* plays now the role of T^* as a hypothetical second-order phase transition temperature located below the clearing point. Warner et al. pointed out that an increase of T^* as predicted by eq 20 should occur only if the network formation is performed in the nematic phase, since this leads to a stabilization of this phase.[15] To the contrary, cross-linking above the clearing point should stabilize the isotropic phase. In this case a lowering of T^* is expected. For the interpretation of our experiments the shift of T^* due to cross-linking plays only a minor role, since we do not compare cross-linked and un-cross-linked systems. So, for reasons of simplicity, we interpret our data in terms of the Landau–de Gennes theory.

In the isotropic phase, where S is small, the third- and fourth-order terms in S in eq 19 can be neglected. Minimizing f then results in the temperature dependence of the equilibrium value of the order parameter in the isotropic phase:

$$S_{eq}(T) = \frac{1}{a(T - T_N^*)}\frac{U}{E}\sigma \quad (21)$$

When T_N^* is approached from high temperatures, the order parameter of the stressed sample shows a critical divergence. Since the birefringence and the static stress-optical coefficient are proportional to S, they show the same critical behavior:

$$\Delta n(T) \approx \Delta n_{max} S_{eq}(T) = \frac{\Delta n_{max}}{a(T - T_N^*)}\frac{U}{E}\sigma \quad (22)$$

$$C(T) = \frac{\Delta n(T)}{\sigma(1 + \epsilon)} = \frac{\Delta n_{max}}{a(T - T_N^*)(1 + \epsilon)}\frac{U}{E} \quad (23)$$

Here Δn_{max} is the birefringence in the case of a perfect alignment state of the mesogens ($S = 1$).

Table II. Parameters Derived from the Fitting of the Spectra of $C^*(\omega)$

		relaxation frequency		relaxation strength		
sample	process	M, 10^{-3} Hz/K	T_N^*, °C	A, 10^{-9} K/Pa	T_N^*, °C	ΔC_0, 10^{-9} Pa^{-1}
LCE-1	slow	26 ± 5	59.0 ● 0.5	249 ± 32	59.0 ± 0.2	37.7 ± 3.8
	fast	923 ● 46	58.5 ± 0.1	152 ● 14	58.1 ± 0.2	1.0 ± 1.5
LCE-5	slow			26 ± 9	61.7 ± 0.7	15.5 ± 0.9
	fast			11 ± 3	60.5 ± 0.5	1.0 ● 0.3

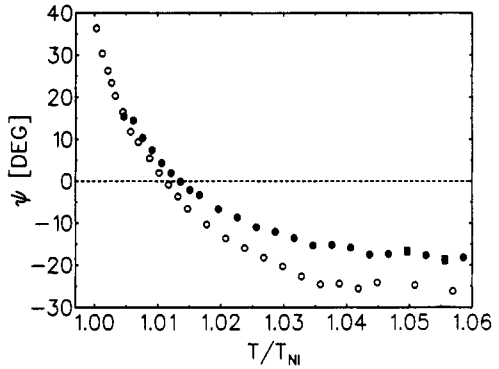

Figure 9. Temperature dependence of the phase shift $\psi = \varphi - \delta$ between strain and birefringence, measured at $f = 3$ Hz. Values greater than zero indicate that the strain signal precedes the birefringence signal.

To describe the dynamical behavior of the order parameter, de Gennes introduced the phenomenological equation[7,16]

$$\frac{\partial S}{\partial t} = -L\frac{\partial f}{\partial S} \tag{24}$$

where L is a phenomenological kinetic coefficient. Inserting the quadratic approximation of eq 19 into eq 24 results in

$$\frac{\partial S}{\partial t} = -La(T - T_N^*)S + \frac{U}{E}L\sigma \tag{25}$$

Equation 25 is solved by

$$S(t) = S_{eq} + (S(t_0) - S_{eq})\exp[-La(T - T_N^*)t] \tag{26}$$

The stress-optical coefficient exhibits the same exponential dynamical behavior. In the frequency domain it shows up as a Debye process with relaxation frequency

$$f_0 = \frac{1}{2\pi}La(T - T_N^*) \tag{27}$$

and a relaxation strength

$$\Delta C = \frac{U}{E}\frac{1}{a(T - T_N^*)} \tag{28}$$

Equation 27 indicates a critical slowing down upon approaching T_N^*. It corresponds to eq 14, which was used in the analysis of the temperature dependence of the experimentally determined relaxation frequencies. The critical divergence of the relaxation strength, expressed by eq 28, is the basis for eq 13, used to fit the measured relaxation strengths. Note that in the derivation of the dynamical behavior the free energy density of eq 19 is used, which is only valid for the equilibrium strain. Hence, the eqs 25–28 are only valid if the strain relaxes on a shorter time scale than the order parameter.

The cross-linking density n_x enters into the Landau–de Gennes theory through E and U. According to de Gennes, the coupling constant U should be proportional to the cross-linking density, as is the case for the elastic modulus E.[6] Hence, one expects an effect of n_x on T_N^*, but no effect of n_x on the relaxation frequencies and relaxation strengths ΔC (only the quotient U/E enters in eqs 21–23, 25, 27, and 28, and this quotient should be independent of n_x).

The reason for the invariance of ΔC with regard to n_x in the Landau–de Gennes model can be understood in a slightly modified description. To characterize the anisotropy of the stretched polymer network, we introduce an orientational order parameter of the backbone segments S_B, defined in analogy to the liquid crystalline order parameter:[17]

$$S_B = \langle P_2(\cos(\theta_B))\rangle = \frac{3}{2}\langle\cos^2(\theta_B)\rangle - \frac{1}{2} \tag{29}$$

Here, P_2 is the second Legendre polynomial and θ_B is the angle between a chain segment and the stretching direction. It is a basic property of ordinary rubbers that the stress-optical coefficient is independent of the cross-linking density.[11,12] Networks with different cross-linking densities experiencing stresses of the same magnitude show the same birefringence and therefore the same backbone order parameter S_B. For the backbone chains in liquid crystalline elastomers in the isotropic phase, the same behavior is expected: the backbone anisotropy should also be independent of the cross-linking density.

Using the order parameters S and S_B, it is reasonable to describe the coupling energy between the backbone segments and the mesogenic side groups by a term

$$f_C = -VSS_B \tag{30}$$

Since f_C is thought to account for the local interaction between the two kinds of segments, the coupling strength V should be independent of the cross-linking density.

De Gennes' assumption $U \sim n_x$ is equivalent to eq 30. This becomes clear by considering first that the relation between backbone order parameter S_B and the strain is given by

$$S_B = \tilde{C}\sigma = \tilde{C}E\epsilon \tag{31}$$

Here $\tilde{C}$ is a constant independent of n_x, which in the case of ordinary rubbers is proportional to the stress-optical coefficient. Using eq 31, the Landau–de Gennes free energy given in eq 17 can be expressed as a function of S and S_B instead of S and ϵ:

$$f = f_0 + \frac{a(T - T^*)}{2}S^2 - \frac{B}{3}S^3 + \frac{C}{4}S^4 - \frac{U}{E\tilde{C}}SS_B + \frac{1}{2}\frac{S_B^2}{E\tilde{C}^2} - \sigma\frac{S_B}{E\tilde{C}} \tag{32}$$

Comparison of the coupling terms in eqs 17 and 32 shows

$$V = \frac{U}{E\tilde{C}} \tag{33}$$

or

$$U = \tilde{C}VE \sim n_x \tag{34}$$

Instead of using eq 17, a discussion of the static and dynamic properties of liquid crystalline elastomers can also be based on eq 32.

Comparison between Theory and Experiment. As predicted by the Landau–de Gennes theory, the relaxation strengths of the reorientation processes diverge and the relaxation rates show a critical slowing down when the temperature approaches T_N^* in the isotropic phase.

Equation 18 explains the lengthening of the sample which accompanies the transition to the nematic phase, shown in Figure 4. Kaufhold et al. have already investigated the validity of eq 18 by static stress-optical measurements and found a good agreement.[1,2]

The appearance of two relaxation processes in the spectra of the stress-optical coefficient may be due to the special coupling of the spacer to the side of the mesogen. In dynamical Kerr effect measurements on liquid crystalline side group polymers of the same general type also two relaxation processes have been reported.[18] The existence of the two processes probably originates from the fact that due to the lateral coupling of the spacer to the mesogen the two short molecular reorientation axes are no longer equivalent. The mesogens behave in a "dynamically biaxial" manner. For a rotation of a mesogen around the short axis "*I*", oriented perpendicular to the spacer axis and the long axis of the mesogenic group, the spacer and a part of the backbone have to join the motion. In contrast to this, a rotation of a mesogen around the short axis "II", oriented parallel to the spacer axis, can take place without a movement of spacer and backbone. Hence, the slow process in the measured spectrum of the stress-optical coefficient could be associated with a rotation of the mesogens around the axis "I", where the backbone causes a slowing down and a broadening of the process; the fast process in the spectrum probably originates from a rotation of the mesogens around the axis "II".

The observed strong dependence of the relaxation strengths on the cross-linking densities is in contrast to the predictions of the Landau–de Gennes theory. A high cross-linking density causes low relaxation strengths. Similarly, the mesaured lengthening of a sample in the nematic phase (Figure 4) is also strongly dependent on cross-linking density. The lengthening of the sample LCE-1 with lower cross-linking density is much larger than the lengthening of the higher cross-linked sample LCE-5. This behavior is also in contrast to a prediction of the Landau–de Gennes theory regarding eq 18. An explanation of the observed dependence on the degree of cross-linking can be offered if it is assumed that the cross-linking points locally perturb the liquid crystalline order. In limited regions around the cross-links the order parameter is greatly reduced. The higher cross-linked sample has more defects and therefore a lower average order parameter. Hence, it shows lower relaxation strengths in the isotropic phase and a smaller lengthening in the nematic phase. On the other hand, as expected in this situation, the relaxation rates remain unchanged.

A second point, which at a first glance does not correspond to the spirit of the Landau–de Gennes theory, is the measured phase angle between strain and birefringence, which is not always positive (see Figure 9). In the Landau–de Gennes theory, a direct coupling ($-\sigma\epsilon$) between the stress σ and the strain ϵ is assumed. The orientational order S of the mesogenic groups and hence the birefringence then result from the interaction of the mesogens with the stretched anisotropic network ($-US\epsilon$). Hence, at first sight it looks unreasonable that the sample becomes birefringent before it is strained. Furthermore, eqs 27 and 28, which are used for the discussion of the measured relaxation frequencies and relaxation strengths, are only valid if the strain of the sample is built up on a shorter time scale than the liquid crystalline order. To overcome these difficulties, a closer look at the mechanical behavior of a sample is necessary. The relaxation process which transforms the sample from the glassy into the rubbery state exhibits a broad time distribution. The short time contributions are associated with the chain motion for fixed chemical and physical junction points in the network, while the long time contributions are mainly related to an entanglement slipping. On applying a constant stress, the anisotropy of the network turns up with the short time contributions, while the entanglement slipping at later times leaves S_B essentially unchanged. This picture is also supported by the results of simultaneous oscillatory mechanical and stress-optical measurements on polymer melts performed by Vinogradov et al.[19] It was observed that stress and birefringence are in phase while the strain is delayed. For non-liquid crystalline samples, the birefringence is a measure for the backbone order parameter, as already mentioned in connection with eq 31. The phase angle between stress and strain and therefore between birefringence and strain shows that there are slow relaxation processes in the mechanical spectrum like the entanglement slipping which do not affect the anisotropy of the temporary network in the melt. In the temperature range of the experiment ($T > T_{NI} = 60$ °C), the mechanical relaxation in the frequency window of the apparatus is dominated by entanglement slipping. Hence, it has nothing to do with the measured stress-optical processes, which are triggered by faster contributions of the mechanical spectrum. Considering this behavior, it appears that the description of the coupling in eq 32 ($-VSS_B$) is more appropriate than the notation as in eq 17 ($-US\epsilon$). The strain contains all contributions of the mechanical spectrum, those of the temporary network and the entanglement slip, whereas only the first ones are relevant.

Conclusion

Two liquid crystalline elastomers with different cross-linking densities were examined by dynamic mechanical and dynamic stress-optical measurements. In the isotropic phase, the spectra of the stress-optical coefficient C^* can be interpreted with the help of two relaxation processes, which can be resolved by fitting the real and imaginary parts of C^* simultaneously. The appearance of two processes is probably due to the lateral coupling of the spacers to the mesogens, which results in a difference in the rotational mobility for the two short axes. Both relaxation processes show critical behavior which is in qualitative agreement with the Landau–de Gennes theory. A higher cross-linking density leads to lower relaxation strengths. This observation is indicative for a perturbation of the liquid crystalline order around the cross-linking points. Only the fast contributions to the mechanical spectrum change the anisotropy of the network and therefore trigger the stress-optical processes. On the other hand, the mechanical process showing up in the frequency window of the experiment appears to be mainly associated with an entanglement slip. It has no effect on the anisotropy of the network and therefore on the liquid crystalline order and the stress-optical coefficient.

Acknowledgment. We thank Dr. W. Kaufhold for providing the characterized samples. Financial support of this work by the Deutsche Forschungsgemeinschaft (Sonderforschungsbereich 60 and Graduiertenkolleg "Strukturbildung in makromolekularen Systemen", Uni-

versität Freiburg) is gratefully acknowledged. We are also grateful for the support provided by the Dr. Otto Röhm Gedächtnisstiftung.

References and Notes

(1) Schätzle, J.; Kaufhold, W.; Finkelmann, H. *Makromol. Chem.* **1989**, *190*, 3269.
(2) Kaufhold, W.; Finkelmann, H.; Brand, H. R. *Makromol. Chem.* **1991**, *192*, 2555.
(3) Landau, L. *Phys. Z. Sowjet.* **1937**, *11*, 26.
(4) de Gennes, P.-G. *Mol. Cryst. Liq. Cryst.* **1971**, *12*, 193.
(5) de Gennes, P.-G. *C. R. Seances Acad. Sci. Paris* **1975**, *281B*, 101.
(6) de Gennes, P.-G. In *Polymer Liquid Crystals*; Ciferri, A., Krigbaum, W. R., Meyer, R. B., Eds; Academic Press: New York, 1982.
(7) de Gennes, P.-G. *The Physics of Liquid Crystals*; Clarendon Press: Oxford, 1986.
(8) Read, B. E. *Polymer* **1964**, *5*, 1.
(9) Hashimoto, T.; Prud'homme, R. E.; Keedy, D. A.; Stein, R. S. *J. Polym. Sci., Polym. Phys. Ed.* **1973**, *11*, 693.
(10) Kyu, T.; Yasuda, N.; Tabushi, M.; Nomura, S.; Kawai, H. *Polym. J.* **1975**, *7*, 108.
(11) Janeschitz-Kriegl, H. *Polymer Melt Rheology and Flow Birefringence*; Springer: Berlin, Heidelberg, 1983.
(12) Treloar, L. R. G. *The Physics of Rubber Elasticity*, 3rd ed.; Clarendon Press: Oxford, 1975.
(13) Cole, K. S.; Cole, R. H. *J. Chem. Phys.* **1941**, *9*, 341.
(14) Warner, M. In *Side Chain Liquid Crystal Polymers*; McArdle, B., Ed.; Blackie and Son: Glasgow, 1989.
(15) Warner, M.; Gelling, K. P.; Vilgis, T. A. *J. Chem. Phys.* **1988**, *88*, 4008.
(16) Doi, M.; Edwards, S. F. *The Theory of Polymer Dynamics*; Clarendon Press: Oxford, 1986.
(17) The introduction of a backbone order parameter is in analogy to the introduction of a backbone order parameter in the description of combined liquid crystalline polymers with mesogenic groups in the backbone and side groups, as described in ref 15.
(18) Hirschmann, H.; Jungbauer, D. A.; Wolf, M.; Wendorff, J. H.; Finkelmann, H.; Hessel, F. *Polym. Adv. Technol.* **1990**, *1*, 93.
(19) Vinogradov, G. V.; Isayev, A. I.; Mustafaev, D. A.; Podolsky, Y. Y. *J. Appl. Polym. Sci.* **1978**, *22*, 665.